Quasi-Periodic Variations of the Polar Vortex in the Southern Hemisphere Stratosphere Due to Wave–Wave Interaction

YASUKO HIO AND SHIGEO YODEN

Department of Geophysics, Kyoto University, Kyoto, Japan

(Manuscript received 20 November 2003, in final form 1 April 2004)

ABSTRACT

The winter polar vortex in the Southern Hemisphere stratosphere is characterized by prominent quasi-stationary planetary waves: zonal wavenumber 1 (wave 1) and the eastward-traveling wave (wave 2). Quasi-periodic variations of the polar vortex are investigated in terms of the wave–wave interaction between wave 1 and wave 2 with both the NCEP–NCAR reanalysis dataset from 1979 to 2002 and a spherical barotropic model.

A typical case shows that the transient wave 1 generated by the wave–wave interaction has comparable amplitude to those of the stationary wave 1 and the traveling wave 2, and has a node around 60°S, where these primary waves have large amplitude. The transient wave 1 travels eastward with the same angular frequency as that of the traveling wave 2. The polar night jet also vacillates with the same frequency such that it has its minimum when the stationary wave 1 and the transient wave 1 are in phase at the polar side of the node. The vacillation is basically due to quasi-periodic variations of the wave driven by the interference between the stationary and traveling wave 1s.

Similar periodic variations of the polar vortex are obtained in the model experiment here, in the circumstance that stationary wave 1 generated by surface topography has comparable amplitude to the eastward-traveling wave 2 that is generated by the barotropic instability of a forced mean zonal wind.

The winter polar vortex shows large interannual variability. Similar quasi-periodic variations due to wave–wave interaction often occurred for the 24 yr in late winter when the transient wave 2 was vigorous.

1. Introduction

In the Southern Hemisphere (SH) stratosphere, quasi-stationary planetary waves of zonal wavenumber 1 (hereafter wave 1) and eastward-traveling wave 2 with a period of about 15 days are prominent in late winter (e.g., Harwood 1975). It has been widely recognized that the quasi-stationary wave 1 is generated in the troposphere due to zonal asymmetry of the surface topography and land–sea distributions, and propagates into the stratosphere (e.g., Randel 1987). Interannual variation of the quasi-stationary wave 1 was investigated by Hio and Hirota (2002). On the other hand, the generation mechanism of the eastward-traveling wave 2 is instability of the polar night jet (Hartmann 1983; Manney et al. 1988). Manney et al. (1991a) found that the wave 2 is confined to the stratosphere during the episodes of its regular eastward propagation, while the wave 2 in the stratosphere is propagated from the upper troposphere during episodes of largest growth. A subsequent eigenvalue analysis (Manney et al. 1991b) also showed that barotropic/baroclinic instabilities play an important role for the generation of the stratospheric wave 2 in late winter. Some other mechanisms for the generation of traveling wave 2 have also been proposed, such as the baroclinic instability of the zonal mean field in the troposphere (Hartmann 1979) and the wave–wave coupling among baroclinic waves (Young and Houben 1989; Scinocca and Haynes 1998).

The importance of wave–wave interaction in the planetary wave variations has been investigated for the Northern Hemisphere (NH) winter since the 1980s. The negative correlation between the amplitude of waves 1 and 2 in the NH stratosphere (e.g., Hirota and Sato 1969) was investigated by calculating the potential enstrophy budget (Smith 1983; Smith et al. 1984; Robinson 1985). As for the SH, wave–wave interaction between stratospheric waves 1 and 2 in late winter and spring has been reported by some authors; Mechoso et al. (1988) and Manney et al. (1991a) suggested that these amplitudes are sometimes anticorrelated in time during September and October.

Hirota et al. (1990) and Shiotani et al. (1990) studied quasi-periodic amplification of wave 1 in the SH stratosphere in late winter and found that the wave-1 amplitude reaches its maximum when the ridges of waves 1 and 2 overlap. Ushimaru and Tanaka (1992) simulated the interaction among wave 1, wave 2, and the zonal mean zonal flow using a semispectral stratosphere-only

Corresponding author address: Yasuko Hio, Department of Geophysics, Kyoto University, Kyoto 606-8502, Japan.
E-mail: hio@kugi.kyoto-u.ac.jp

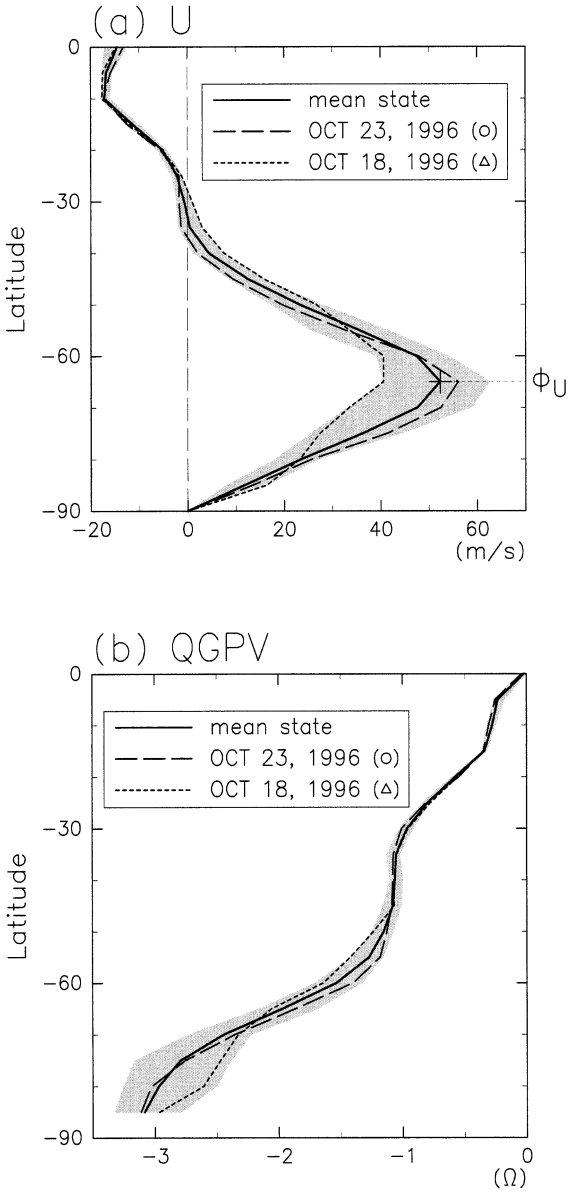

FIG. 1. (a) Latitudinal profiles of zonal mean zonal wind and (b) zonal mean QGPV at 20 hPa for the 20-day period from 8 to 27 Oct 1996. The solid line shows the time mean state along with the variation range (shaded region). The broken and dashed lines show the profiles on 23 and 18 Oct respectively. The value of the QGPV is scaled by the rotation rate of the earth $\Omega = 7.292 \times 10^{-4}\ \mathrm{s}^{-1}$.

model in which both the stationary wave 1 and the eastward-traveling wave 2 were prescribed at the bottom boundary near the tropopause. In their model result, the energy transfer between wave 1 and wave 2 is important for the periodic amplification of wave 1.

Some model studies have shown that stratospheric variations, such as the vacillation of the mean zonal flow, can occur internally with fixed external conditions, including time-independent wave forcing near the tropopause (e.g., Holton and Mass 1976; Yoden 1987; Scaife and James 2000). The vacillation phenomenon corresponds to periodic occurrence of the stratospheric sudden warming events. All of their results show the importance of the periodic change in the vertical structure of the polar vortex through the Rossby wave–mean flow interactions. Recently, Rong and Waugh (2004, hereafter RW) examined internal variability of the polar vortex in a shallow water model, that is, a one-layer model, with time-independent topographic forcing and relaxation to a constant zonally symmetric equilibrium state. They demonstrated that the horizontal structure of potential vorticity (PV) as well as the vertical structure plays an important role in the vacillation of the stratospheric flow. For the large topographic amplitude, there are breakdown and recovery cycles of the polar vortex, and filamentary structures are produced during the vortex breakdown due to a highly nonlinear process.

For the small amplitude forcing cases in the RW experiments, on the other hand, there is only a periodic undulation of the edge of the polar vortex and the vacillation of the mean zonal flow does not occur. These features resemble the SH winter circulation. In contrast to RW, we focus on the periodic variations under such a condition that the flow obeys the weakly nonlinear dispersion theory. This condition allows a triad of wavenumbers for resonant energy exchange (Lighthill 1978). Under the circumstance of the SH winter stratosphere, the stationary wave 1 [$A_1 \exp(\mathbf{k}_1 \cdot \mathbf{x})$] and the eastward-traveling wave 2 [$A_2 \exp(\mathbf{k}_2 \cdot \mathbf{x} - \omega_2 t)$] of the same latitudinal harmonics can generate traveling waves 1 or 3 [$A_3 \exp(\mathbf{k}_3 \cdot \mathbf{x} - \omega_3 t)$], which satisfy the following relationships:

$$\mathbf{k}_1(1, l) + \mathbf{k}_2(2, l) = \mathbf{k}_3(1 \text{ or } 3, 2l), \quad (1)$$

$$0 + \omega_2 = \omega_3. \quad (2)$$

Therefore, a higher harmonic wave 1 or 3, which has the same angular frequency as the traveling wave 2 (ω_2), may be generated by the wave–wave interaction. However, to our knowledge, there is no study on the horizontal structure variations concerning the wave–wave interaction in the SH stratosphere.

This work aims to investigate quasi-periodic variations of the polar vortex through wave–wave interactions between wave 1 and wave 2, using the National Centers for Environmental Prediction–National Center for Atmospheric Research (NCEP–NCAR) reanalysis dataset. We use the daily data for 24 yr from 1979 to 2002 as Hio and Yoden (2005). Waves are divided into a stationary (time averaged) component and a transient (deviation from the time mean) component, and time variations of their horizontal structures are studied to capture the nature of the wave–wave interactions. We also use a spherical barotropic model to understand the dynamical elements that produce such periodic variations of the polar vortex.

A detailed analysis for a typical example of the observed wave–wave interactions will be shown in the

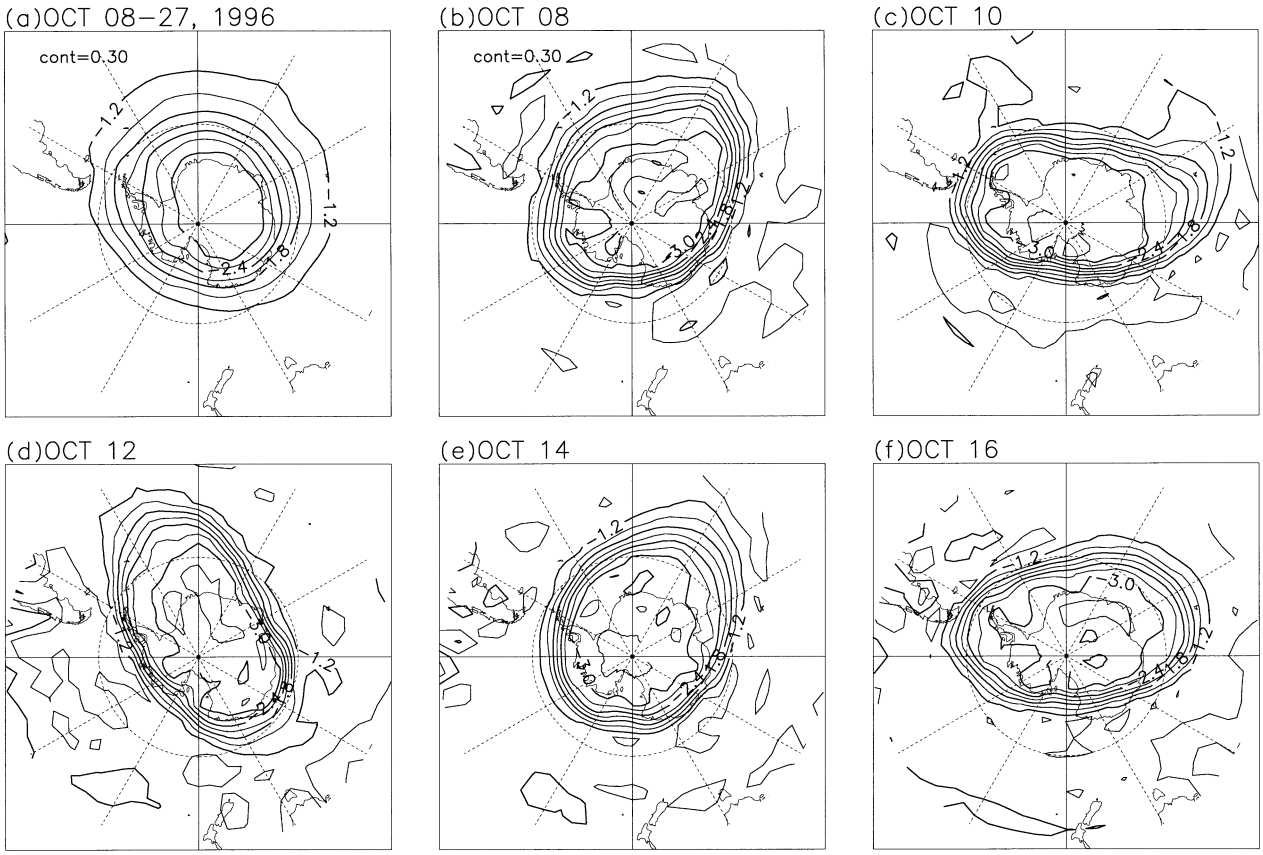

FIG. 2. (a) QGPV field at 20 hPa averaged for the 20-day period from 8 to 27 Oct 1996 and (b)–(f) its time evolution on the poleward side of 35°S. The value is scaled by Ω and the contour interval is 0.3.

next section, and the result of the model experiment similar to the observation is described in section 3. In section 4, the interannual variations of the wave–wave interactions are investigated. Discussion is in section 5, followed by the conclusions in section 6.

2. A typical case in October 1996

In this section, we focus on a typical period for the 20 days from 8 to 27 October 1996, during which quasi-periodic variations of the polar vortex were observed clearly.

a. Latitudinal structure of zonal mean states

Figure 1a shows the latitudinal profile of the time-averaged zonal mean zonal wind $\langle\overline{u}\rangle$ (solid line) in the SH at 20-hPa level for this period, where $\langle A\rangle$ denotes the time mean of A and $\overline{A}$, the zonal mean. The maximum speed of the polar night jet exceeds 50 m s^{-1} at 65°S where the time variation (shaded region) is also the largest. The latitudinal profile of the time-averaged zonal mean quasigeostrophic PV (hereafter QGPV) $\langle\overline{q}\rangle$ at 20 hPa (Fig. 1b) shows a monotonic increase with latitude ϕ. It is nearly constant in midlatitudes in contrast to the large gradient ($\partial\langle\overline{q}\rangle/\partial\phi$) in the high latitudes around the latitude of the jet core. Broken and dashed lines indicate these profiles when the zonal mean zonal wind is strong (23 October) or weak (18 October) at 65°S, respectively. The zonal mean zonal wind on 23 October is stronger than that on 18 October in the high latitudes, whereas it is weaker on the equator side of 55°S. Corresponding to this, $\partial\langle\overline{q}\rangle/\partial\phi$ on 23 October is larger than the time mean state in the high latitudes and slightly negative in the midlatitudes around 40°S, while on 18 October it is smaller than the mean state in the high latitudes and nearly zero in the midlatitudes.

b. Horizontal patterns

Figure 2a shows the time mean state of the QGPV field at 20 hPa for the 20 days. The polar vortex is displaced off the Pole with a circular pattern, indicating the dominance of wave 1 for the stationary component. As to the time evolution (Figs. 2b–f), the elongated polar vortex rotates eastward with a period of about 6 days, changing its shape quasi-periodically. The polar vortex on 8 October is roughly circular, and it is stretched along 90°E–90°W lines on 10 October. After that, it becomes less elongated, and its shape on 14 October is roughly

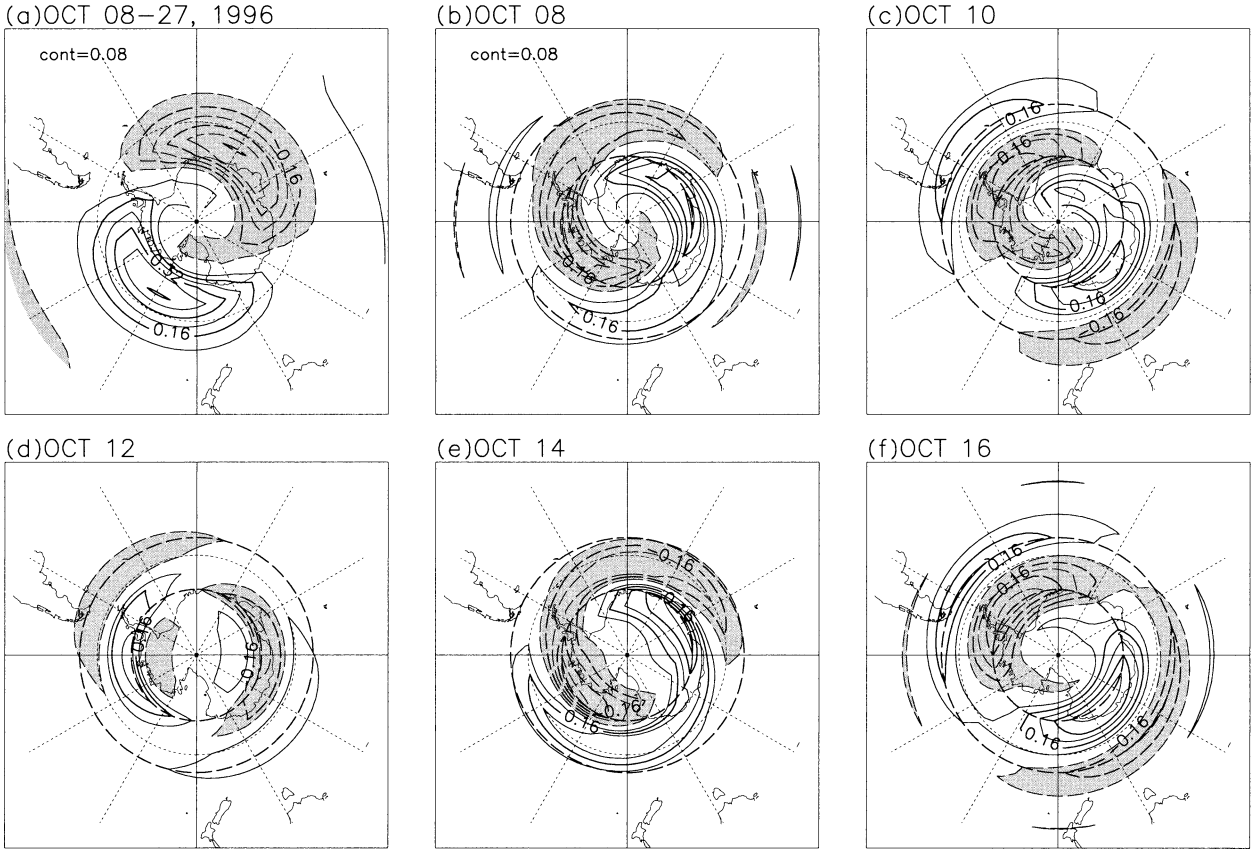

FIG. 3. (a) Vorticity field of the stationary wave 1 at 20 hPa and (b)–(f) time evolution of the transient wave 1 for the 8-day period from 8 to 16 Oct 1996. The value is scaled by Ω and the contour interval (cont) is 0.08. Zero lines are not drawn and the areas where the value is smaller than $-$cont are shaded.

circular again similar to that on 8 October. These quasi-periodic variations are observed throughout the analyzed 20 days.

Eddies ($A' = A - \overline{A}$) are divided into stationary waves defined as zonal asymmetries in the time means ($\langle A' \rangle$) and transient waves defined as the deviations from the time means ($A'^* = A' - \langle A' \rangle$), and Fourier decomposition is taken in longitudes to obtain their component for each zonal wavenumber. Horizontal patterns of wave 1 and wave 2 are displayed in Figs. 3 and 4, respectively. The stationary wave 1 (Fig. 3a) has much larger amplitude than the stationary wave 2 (Fig. 4a), and has its maximum at 65°S. Transient wave 2 (Figs. 4b–f), which has a much larger amplitude than the stationary component, rotates eastward with the phase speed of about 30° day^{-1}, corresponding to the rotation of the elongated polar vortex (Figs. 2b–f). During 8–12 October (Figs. 4b and 4d), the phase tilt with latitude of the transient wave 2 changes from southeast–northwest to southwest–northeast. Opposite variation of the phase tilt is also seen from 12 to 16 October.

Transient wave 1 (Figs. 3b–f) rotates eastward with a period of about 6 days. It has comparable amplitude to the stationary wave-1 component and has a nodal structure in latitudes with a secondary maximum in mid-latitudes. The dashed lines in Fig. 3 indicate the latitudes at which the time mean amplitude of the transient wave 1 has local maximum, 70° and 55°S. On 8 (Fig. 3b) and 14 October (Fig. 3e), the transient wave 1 shifts poleward, while it shifts equatorward on 10 (Fig. 3c) and 16 October (Fig. 3f). The phase tilt of wave 1 also changes periodically. On 8 and 14 October, the phase tilts from southwest to northeast, while it does quite slightly on 10 and 12 October. Hereafter, we call transient wave 1 ''traveling wave 1'' and transient wave 2 ''traveling wave 2'' to specify the characteristics of the waves.

c. *Time mean spatial structure*

Time mean structures of the dominant waves are displayed in Fig. 5. The vertical structure of stationary wave 1 at 65°S (Fig. 5a bottom) reveals westward phase tilt with height above 100 hPa, indicating upward propagation of the stationary wave 1 in the lower stratosphere. To illustrate the structure of the traveling waves 1–3, composites for the 20-day data are made by shifting the sections zonally so as to align the wave phase at a

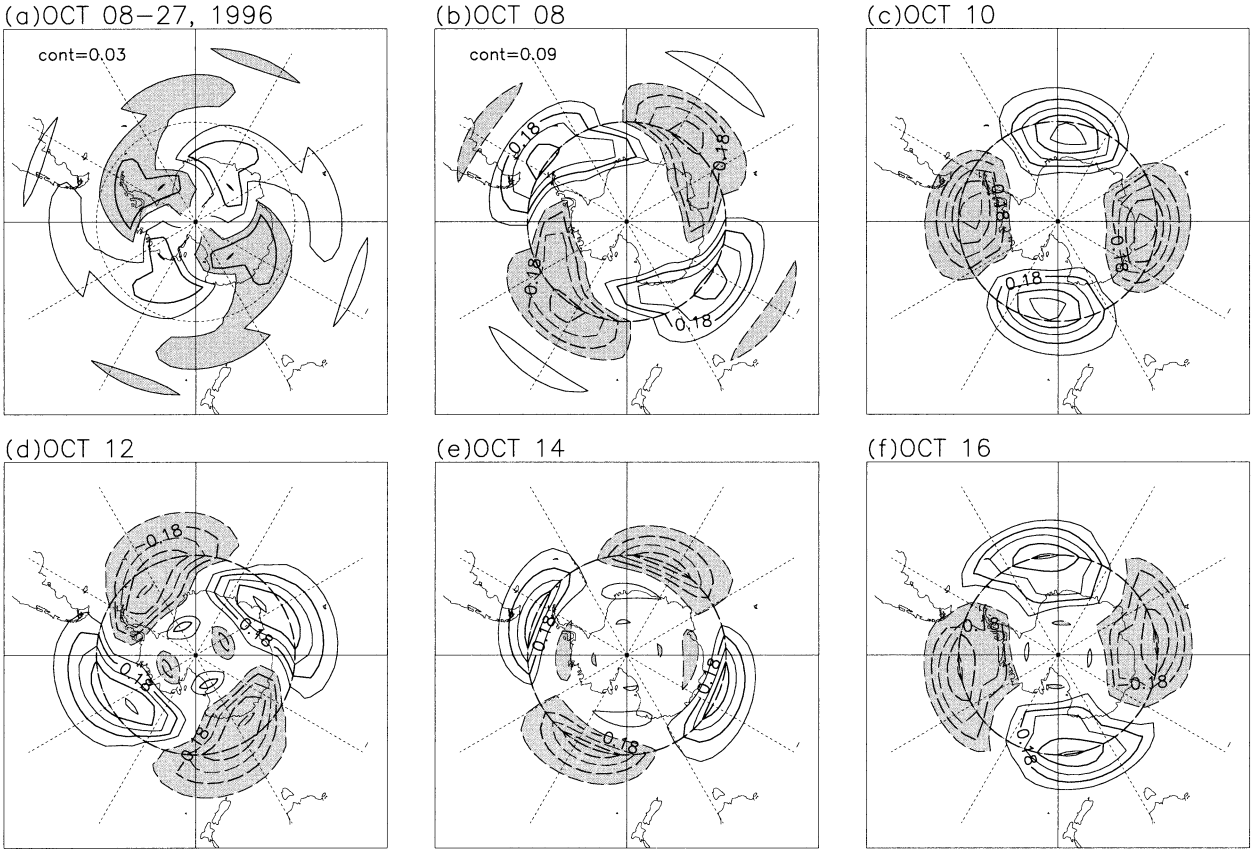

FIG. 4. Same as in Fig. 3, but for wave 2. The contour intervals (cont) are 0.03 for the stationary wave and 0.09 for the transient wave. Zero lines are not drawn and the areas where the value is smaller than −cont are shaded.

reference latitude at 20-hPa level (Figs. 5b–d). We select the reference at the latitude where the time mean amplitude of each wave is maximum at that level: 70°S for wave 1, 60°S for wave 2, and 60°S for wave 3. The characteristics shown here are obtained in case that the reference level is selected above 150 hPa, while not obtained when the reference level is set in the upper troposphere. The composite of traveling wave 2 has a phase tilt from southeast to northwest and is roughly equivalent barotropic between 30 and 10 hPa, while it tilts westward with height between 150 and 50 hPa. The composite of traveling wave 1 has a node around 62.5°S, between the maximum latitude of the stationary wave 1 and that of the traveling wave 2, with the maxima at 70° and 55°S; the amplitude in the Pole side is much larger. The traveling wave 1 has phase tilt from southwest to northeast contrary to the wave 2 and is roughly equivalent barotropic in the stratosphere. The composite of traveling wave 3 also shows a nodal structure with the maxima at 75° and 60°S. The latitudinal structures of the traveling waves 1 and 3 satisfy the relation of Eq. (1); the traveling waves 1 and 3 with a node can be regarded as higher harmonic waves generated by wave–wave interaction between the stationary wave 1 and the traveling wave 2.

The Eliassen–Palm (EP) flux vector represents the wave structure more quantitatively. For wave fields satisfying the quasigeostrophic conditions, the EP flux vector $\mathbf{F}(\phi, p, t) = (0, F_\phi, F_p)^{\mathrm{T}}$ are described as the products of the stationary ($\langle A\rangle$) and transient (A^*) components:

$$\mathbf{F}(\phi, p, t) = \sum_{k=1}^{\infty} \mathbf{F}_k = \sum_{k=1}^{\infty} \begin{pmatrix} 0 \\ F_{\phi_k} \\ F_{p_k} \end{pmatrix}$$

$$= \sum_{k=1}^{\infty} \begin{bmatrix} \rho_0 a \cos\phi(\overline{\langle u_k\rangle\langle v_k\rangle} + \overline{\langle u_k\rangle v_k^*} \\ \qquad + \overline{u_k^*\langle v_k\rangle} + \overline{u_k^* v_k^*}) \\ \rho_0 a \cos\phi \dfrac{f}{\theta_{0z}}(\overline{\langle\theta_k\rangle\langle v_k\rangle} + \overline{\langle\theta_k\rangle v_k^*} \\ \qquad + \overline{\theta_k^*\langle v_k\rangle} + \overline{\theta_k^* v_k^*}) \end{bmatrix},$$

$$= \sum_{k=1}^{\infty} (\mathbf{F}_k^{\langle\rangle\langle\rangle} + \mathbf{F}_k^{\langle\rangle *} + \mathbf{F}_k^{*\langle\rangle} + \mathbf{F}_k^{**}), \qquad (3)$$

where subscript k for each quantity denotes the component associated with zonal wavenumber k, and the other notations are same as Andrews et al. (1987). The EP flux vector for the wave of the zonal wavenumber

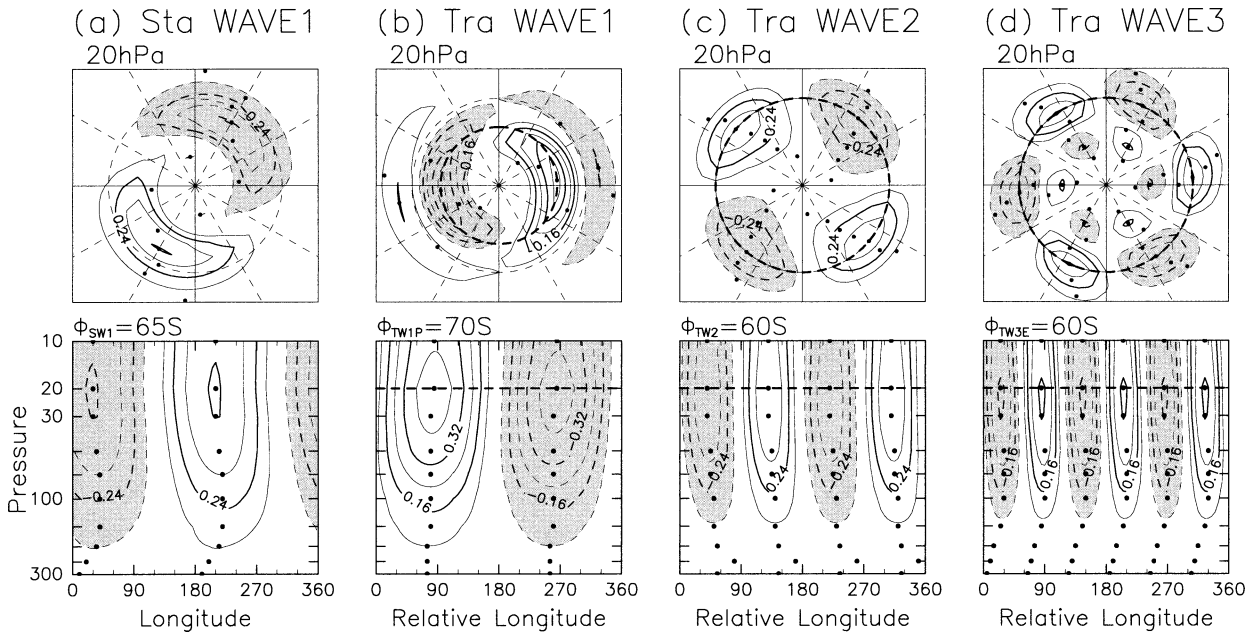

FIG. 5. (a) Time-averaged horizontal structure of stationary wave 1 and (b) transient wave 1, (c) wave 2, and (d) wave 3 (top) at 20 hPa for the 20-day period from 8 to 27 Oct 1996. Reference latitudes for traveling waves to make composite are selected at 70°, 60°, and 60°S, respectively, where the time mean amplitude is maximum at the 20-hPa level and drawn with the dashed lines. (bottom) The vertical structure of the stationary wave 1 at 65°S, and the composite vertical structures of traveling waves 1, 2, and 3 at the reference latitude are shown. The contour intervals (cont) are 0.12 for stationary wave 1 and traveling wave 2, and 0.08 for traveling wave 1 and wave 3. Zero lines are not drawn and the areas where the amplitude is smaller than −cont are shaded.

k, $\mathbf{F}_k = (0, F_{\phi_k}, F_{p_k})^T$, is divided into four components: $\mathbf{F}_k^{\langle\rangle\langle\rangle}$ and $\mathbf{F}_k^{**}$ arise from the stationary and transient wave components, respectively, while $\mathbf{F}_k^{\langle\rangle *}$ and $\mathbf{F}_k^{*\langle\rangle}$ arise from cross terms between these components. As $\langle \mathbf{F}_k^{\langle\rangle *} \rangle = \langle \mathbf{F}_k^{*\langle\rangle} \rangle = \mathbf{0}$, $\langle \mathbf{F}_k^{**} \rangle$ is a rough measure of the time-averaged activity of the transient waves of zonal wavenumber k, and the ratio of the horizontal and vertical components give a measure of the relative importance of barotropic and baroclinic processes associated with each traveling wave.

Figure 6 shows the latitude–height sections of $\langle \mathbf{F}_k^{**} \rangle$ and its divergence for $k = 1$ (Fig. 6b), $k = 2$ (Fig. 6c), and $k = 3$ (Fig. 6d) together with that of the time mean zonal mean zonal wind $\langle \overline{u} \rangle$ (Fig. 6a). Note that the divergence is a wave driving of the zonal mean zonal angular momentum per unit volume: $\rho a \cos\phi(\partial \overline{u}/\partial t) = \nabla \cdot \mathbf{F}$. In the middle stratosphere, there are common features for waves 1–3 that the horizontal components are prominent in high latitudes and that the divergences have dipole structures. In case the traveling waves are not propagated from the troposphere, but are generated in the stratosphere, dominance of the horizontal component of the EP flux is expected for each wave. The EP flux vector for the traveling wave 2 directs equatorward with a node of the dipole pattern on the equator side of the jet core (Fig. 6a), suggesting the importance of barotropic instability. The horizontal dipole of the wave driving confined in the stratosphere is a typical pattern for wave 2 reported in previous papers in the monthly mean fields in winter and spring (e.g., Hartmann et al. 1984; Manney et al. 1991a). As for the traveling wave 1, the EP flux (Fig. 6b) directs poleward, and the wave driving has the opposite sign in high latitudes. The EP flux vector for wave 3 (Fig. 6d) directs equatorward on the equator side of the jet core and poleward on the Pole side in the middle stratosphere. The EP flux vectors in the lowermost stratosphere for traveling waves 2 and 3 seem to be related to the tropospheric wave activity, but we focus only on the middle stratosphere around 20 hPa in this paper.

d. Time variations

Figures 7a–d show Hovmöller diagrams at the 20-hPa level for traveling wave 1 at 55° and 70°S, traveling wave 2 at 60°S, and traveling wave 3 at 60°S. At these latitudes, each traveling wave has a (local) maximum in the time mean amplitude. The eastward-traveling wave 1 has the same phase speed of about (360/7)° day^{-1} and has a nodal structure with out-of-phase relationship between the lower and higher latitudes. The phase speed of the eastward-traveling wave 2 is about a half of that of wave 1, that is, about (360/14)° day^{-1}, while that of wave 3 is about one third, (360/21)° day^{-1}. In other words, the periods are the same for these traveling waves 1, 2, and 3 (about 7 days). Vertical dashed lines indicate the longitude of the ridge of the stationary wave 1 at 65°S and the mark "×" denotes the timing when the

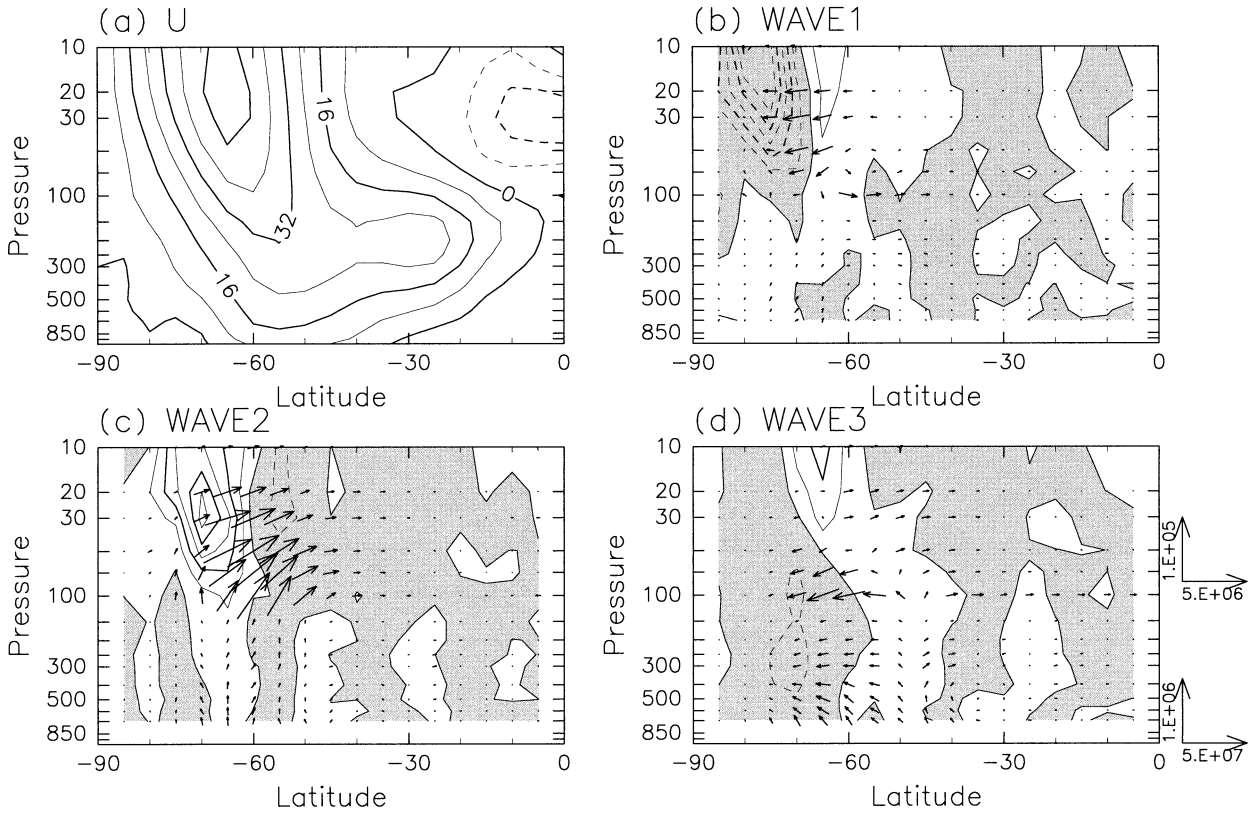

FIG. 6. (a) Latitude–height sections of the time mean zonal mean zonal wind $\langle \overline{u} \rangle$ at for the 20-day period from 8 to 27 Oct 1996, and the time mean EP flux vector consisting of the traveling component $\langle \mathbf{F}^{**} \rangle$ and its divergence expressed as a wave driving of zonal mean zonal angular momentum per unit mass for (b) wave 1, (c) wave 2, and (d) wave 3. The contour interval for $\langle \overline{u} \rangle$ is 8 m s^{-1} and dashed lines indicate negative value. The contour interval for the wave driving is 0.8 m s^{-1} day^{-1} and negative values are shaded. (d) The length of the unit vector is displayed on the right-hand side of the graph. Note that the scaling of the unit vector below 100 hPa is 10 times as large as that at and above 100 hPa.

ridge of the traveling wave 2 at 60°S overlaps with the stationary wave 1 at 65°S. The overlap of the ridge among the traveling wave 1 at 70°S, the traveling wave 2 at 60°S, and the stationary wave 1 occurred at the same time. On the other hand, the trough of the traveling wave 1 at 55°S and that of the traveling wave 3 at 60°S overlap with the ridge of the stationary wave 1 at the same time as denoted by ×. At that time, the traveling waves 2 and 3 tend to have those maximum amplitudes, while the traveling wave 1 tends to have its minimum amplitude.

The zonal mean zonal wind at 65°S at 20 hPa (solid line in Fig. 7e) vacillates with the same period so as to have its minimum value roughly at the same time of the phase overlap. Note that the out-of-phase relationship between the jet core and the midlatitude flank of the jet is seen in broken and dashed lines in Fig. 1 for the two dates when $\overline{u}_{|60°S}$ is strong (denoted by ○) or weak (△).

Another way to show the periodic change of traveling waves more quantitatively is the polar diagram of the complex amplitude of each wave (e.g., Salby and Garcia 1987). The vorticity field can be decomposed in Fourier series with zonal wavenumber k:

$$\zeta = \sum_{k=0}^{K} \mathrm{Re}[\zeta_k(\phi, p, t) \exp(ik\lambda)]$$

$$= \zeta_0(\phi, p, t) + \sum_{k=1}^{K} [|\zeta_k(\phi, p, t)| \cos(k\lambda - k \arg[\zeta_k])]. \quad (4)$$

Figures 8a–c shows the trajectory of $\zeta_k(\phi_i, p_j, t)$ for given ϕ_i and p_j in a Re[ζ_k]–Im[ζ_k] plane, and $|\zeta_k|$ means the amplitude of the wave, and arg[ζ_k] means its phase. In Fig. 8a the total wave vector ζ_1(55°S, 20 hPa, t) is decomposed as the stationary wave-1 vector $\langle \zeta_1$(55°S, 20 hPa)$\rangle$ plus the traveling wave-1 vector ζ_1^* (55°S, 20 hPa, t) (i.e., $\zeta_1 = \langle \zeta_1 \rangle + \zeta_1^*$). The stationary wave 1 at 65°S is indicated by the asterisk mark in Fig. 8b, and half lines passing through the square point of $\langle \zeta_1 \rangle$ in Figs. 8a and 8b have the same phase of the stationary wave 1. The dashed line in Fig. 8c also shows the phase angle of the stationary wave 1 in the polar diagram of wave 2 (2 arg $\langle \zeta_1 \rangle$). The phase relationship seen in

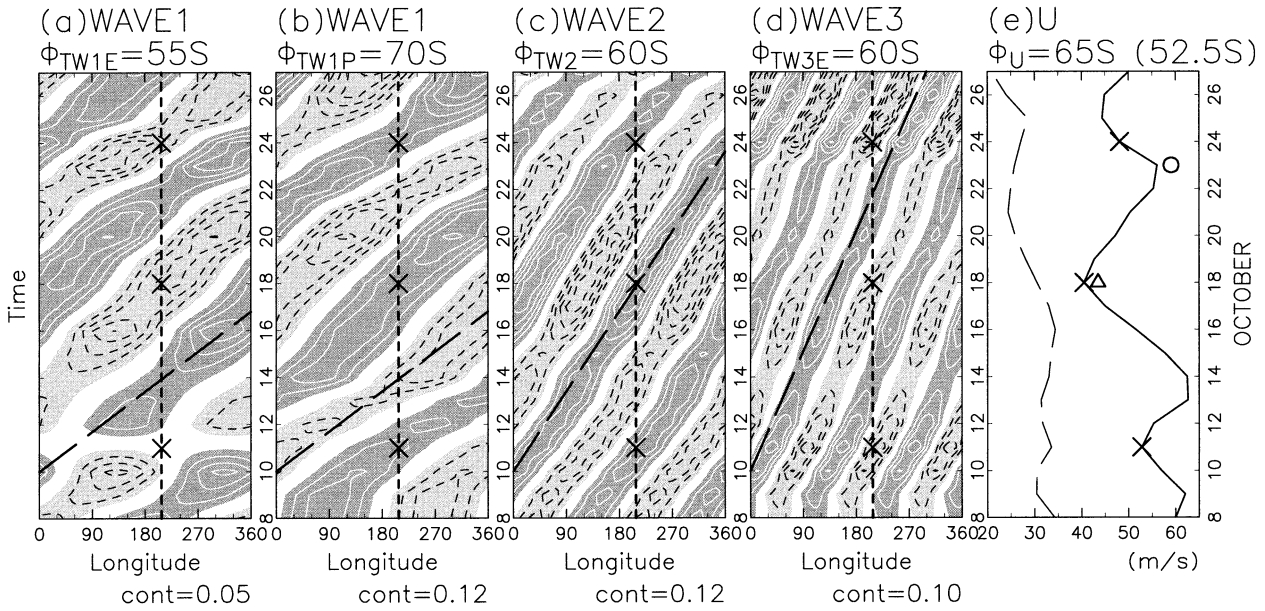

FIG. 7. Hovmöller diagrams of the (a) traveling wave 1 at 55°S and (b) at 70°S, (c) wave 2 at 60°S, and (d) wave 3 at 60°S for vorticity field at 20 hPa for the 20-day period from 8 to 27 Oct 1996. The vertical dashed line indicates the location of the ridge of the stationary wave 1 at 65°S and the mark "×" denotes the time when the ridge of the traveling wave 2 at 60°S overlaps with the stationary wave 1 at 65°S. The value is scaled by Ω and the contour intervals (cont) are denoted under each panel. Dark shade indicates values above cont and light shade below −cont. (e) Time evolutions of the zonal mean zonal wind at 65° (solid line) and 52.5°S (dashed line) are also shown, and the circle and triangle marks indicate the days of which the latitudinal structure is displayed in Fig. 1.

Fig. 7 can be reconfirmed. The traveling components of waves 1 and 2 rotate counterclockwise with the period of about 7 days, (or roughly three rotations for 20 days.) The phase difference between the traveling wave 1 at 70° and that at 55°S is always about π, indicating the out-of-phase relationship between the two latitudes. (Note 6 particular days denoted with the same black or gray numbers.) The traveling wave-1 vector at 70°S and wave-2 vector at 60°S are almost parallel to the stationary wave-1 vector at the same time (dates in gray numbers), and the traveling wave-1 vector at 55°S is almost antiparallel, indicating the same timing of the overlap of these waves.

These polar diagrams enable us to capture the amplitude information more easily. Figures 8a and 8b show the traveling wave-1 component is comparable to the stationary wave 1. The orbits of the total wave 1 are elongated in a direction perpendicular to the stationary wave-1 vector, indicating that the traveling wave 1 has its minimum amplitude when it is in phase or out of phase with the stationary wave 1 and has its maximum amplitude when the phase difference between the stationary wave 1 and the traveling wave 1 is about $\pm\pi/2$. If we see the amplitude variation of the total wave at high latitudes, the amplitude of wave 1 (Fig. 8b) has its maximum when the overlap of these waves takes place (dates in gray numbers), which is consistent with the earlier studies by Hirota et al. (1990) and Shiotani et al. (1990). The amplitude of the total wave 2 (Fig. 8c), which is dominated by the traveling component, also tends to be the maximum when the traveling wave 2 is in phase with the stationary wave 1. The time variation of zonal mean zonal wind at 65°S is shown in Fig. 8d again to confirm that it is weakest when the traveling wave 1 at 70°S is in phase with the stationary wave 1, while it is strongest when the traveling wave 1 at 70°S is in opposite phase to the stationary wave 1.

Quasi-periodic variations of the phase tilt of waves 1 and 2 as shown in Figs. 3 and 4 suggest that the EP flux also fluctuates quasi-periodically. Figure 9a shows the time change of the EP flux for wave 1 ($\mathbf{F}_1$) and its divergence at 20-hPa level. The horizontal component F_{ϕ_1} is relatively large in high latitudes and changes its direction quasi-periodically associated with the phase relation between the stationary wave 1 and the traveling wave 1. Corresponding to this feature, the dipole pattern of the divergence with a node around 60°S also changes its sign quasi-periodically. The divergence or convergence has peaks around 70° or 55°S, where the amplitude of the traveling wave 1 is maximum, at the timing that the amplitude of the traveling wave 1 is maximum (i.e., the traveling wave 1 vector is perpendicular to the stationary wave 1 vector). Interference between the stationary wave and a monochromatic traveling wave can produce this kind of periodic fluctuation of the EP flux (cf. Salby and Garcia 1987). An example of the interference between a normal mode Rossby wave known as "5-day wave" and the forced stationary planetary wave was reported by Hirooka (1986). The dominance of the terms $\mathbf{F}_1^{\langle\rangle}*$ and $\mathbf{F}_1^{*\langle\rangle}$ in $\mathbf{F}_1$ (not shown) is the

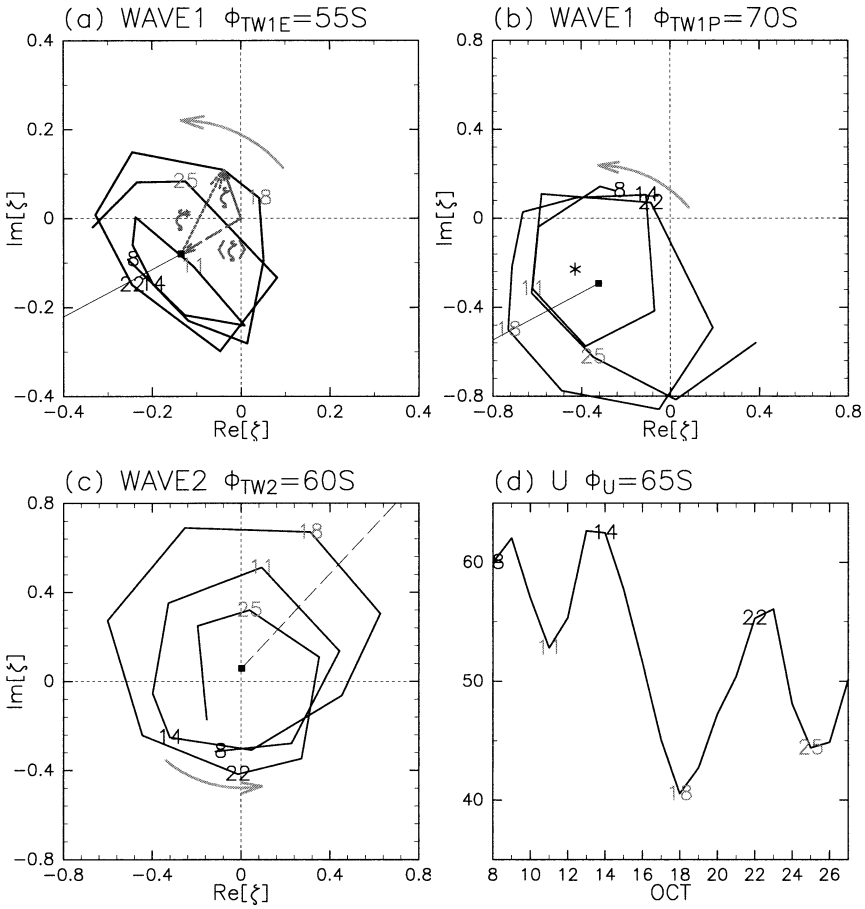

FIG. 8. Polar diagrams of the complex amplitude of wave 1 (a) at 55° and (b) at 70°S, and wave 2 (c) at 60°S at 20 hPa for the selected 20 days. Square marks (■) indicate the stationary component (i.e., the time mean value). The asterisk mark (*) indicates the stationary component of wave 1 at 65°S, and the thin lines passing through the square mark in (a) and (b) and the dashed line in (c) are the phases of the stationary wave 1. (d) Time evolution of the zonal mean zonal wind at 65°S is also shown. Labels correspond to the dates when the traveling wave 1 at 70°S is in phase (black) or out of phase (gray) with the stationary wave 1 at 60°S.

evidence that the interference between the stationary wave 1 and the induced traveling wave 1 by wave–wave interaction causes the quasi-periodic variation of the EP flux. A hint of similar periodicity is also seen for $\mathbf{F}_3$ (Fig. 9c). It points to the same direction as $\mathbf{F}_1$, though the dipole pattern of the divergence is not clearly seen.

As for the wave 2 (Fig. 9b), the horizontal component is dominant for this period except for the 3 days from 16–18 October. For the first half of the period, $\mathbf{F}_2$ also changes its direction rather periodically in the opposite direction to $\mathbf{F}_1$ with the dipole pattern of the divergence of $\mathbf{F}_2$. As the EP flux divergence of the wave-1 component dominates, the total EP flux divergence for waves 1–3 (Fig. 9d) also fluctuates quasi-periodically, which is consistent with the vacillation of the zonal mean zonal wind (Fig. 7e). The EP flux divergence at 65°S precedes the zonal wind by a quarter period. The anticorrelation of the zonal mean zonal wind between 65° (solid line) and 52.5°S (dashed line) shown in Fig. 7e can be explained by the dipole structure of the EP flux divergence mainly due to the interference between the stationary wave 1 and the traveling wave 1, which was generated by the wave–wave interaction between the stationary wave 1 and traveling wave 2.

3. A numerical experiment

a. Model description

We use a dynamical model of the two-dimensional flow on the earth with zonal-flow forcing, dissipation, and surface topography to investigate the fundamental mechanism of the quasi-periodic variation of the polar vortex due to wave–wave interaction described in the previous section. The detailed result will be reported in a separate paper. The flow is governed by a vorticity equation in the form

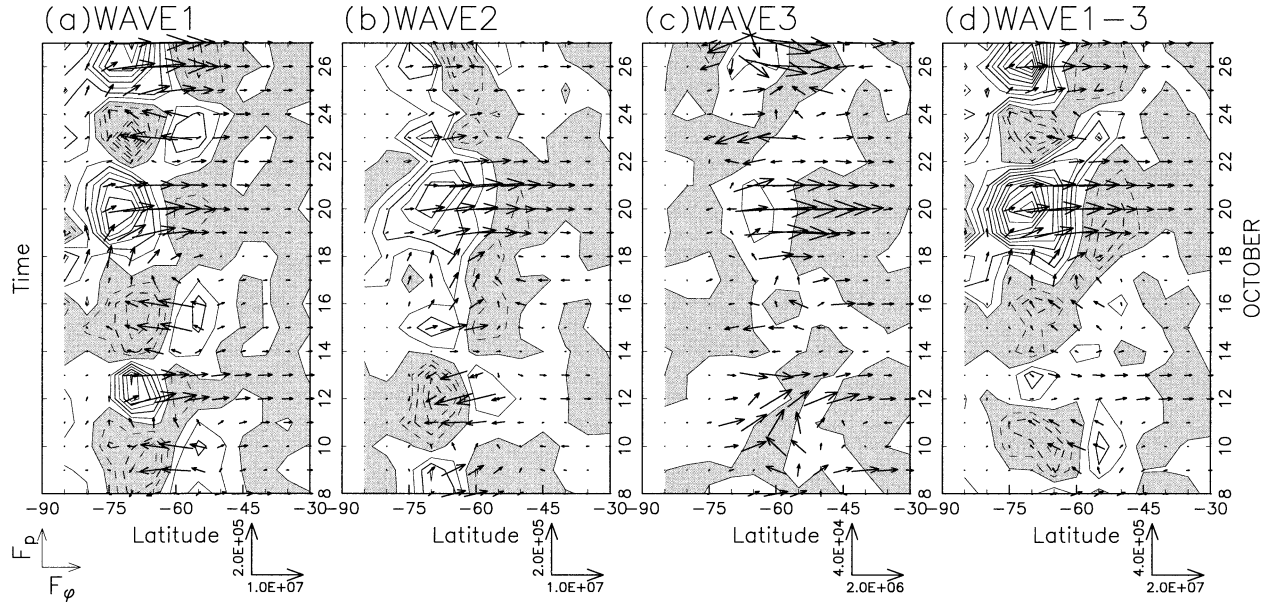

FIG. 9. Latitude–time sections of the EP flux and its divergence expressed as the zonal force per unit mass for (a) wave 1, (b) wave 2, (c) wave 3, and (d) waves 1–3 at 20 hPa for the selected 20 days. The length of the unit vector is displayed under each graph. The contour interval is 0.8 m s^{-1} day^{-1} and negative values are shaded.

$$\frac{D}{Dt}\left(\zeta + f + \frac{hf}{H}\right) = -\alpha(\zeta - \overline{\zeta_0}) + \nu\left(\nabla^2 + \frac{2}{a^2}\right)(\zeta - \overline{\zeta_0}), \quad (5)$$

where $\zeta = \nabla^2\psi$ is the relative vorticity, $f = 2\Omega \sin\phi$ is the Coriolis parameter, Ω is the rotation of the earth, h is the height of the surface topography, and H is the thickness of the fluid layer. The potential vorticity $q = \zeta + f + (hf/H)$ is conserved following fluid motion if the forcing and dissipation terms on the right-hand side of Eq. (5) can be neglected. The relaxation time α^{-1} of the forcing is set to 10 days and the viscosity coefficient ν is fixed at a small constant to give the dissipation time of 1 day at the largest total wavenumber ($N = 85$) as in Mizuta and Yoden (2001). In the SH, sinusoidal surface topography of zonal wavenumber 1 is assumed in longitudinal direction as

$$h(\lambda, \phi) = \frac{1}{2}h_0(\sin 2\phi)^2 \cos\left(\lambda - \frac{\pi}{6}\right), \quad (6)$$

and there is no topography in the NH. The prescribed equilibrium state for the forcing that is given by zonally symmetric vorticity $\overline{\zeta_0} = -(1/a)(\partial\overline{u_0}/\partial\phi)$ is set so as to satisfy the necessary condition of barotropic instability (Hartmann 1983):

$$\overline{u_0} = \frac{1}{2}U\left(1 + \tanh\frac{\phi - \phi_0}{B}\right)\cos\phi, \quad (7)$$

where U is a measure of the intensity of the prescribed jet, B is its width, and ϕ_0 is its position.

The regime diagram in the case without the topography ($h_0 = 0$) was obtained by Ishioka and Yoden (1995). An eastward-traveling wave 2 with constant amplitude is obtained over a wide range of the parameters. We set $U = 240$ m s^{-1} and $\phi_0 = 55°$, and sweep the parameters B and h_0. The regime diagram will be shown in the next paper. At specific parameter ranges, the stationary wave 1 generated by the topography is dominant, as well as the eastward-traveling wave 2 due to barotropic instability, and a periodic variation of the polar vortex occurs in the result of the interaction between these waves. In this section, we examine a result for the parameters $B = 6$ and $h_0/H = 0.08$ as an example of such a situation similar to the observed quasi-periodic variation as described in the previous section.

b. A case similar to observation

Figure 10 shows latitudinal profiles of the time-averaged zonal mean zonal wind $\langle\overline{u}\rangle$ and PV $\langle\overline{q}\rangle$ (solid line) together with the prescribed zonally symmetric forcing (dotted line). Qualitatively similar features as the observation (Fig. 1) are found in mid- and high latitudes except that the jet is stronger. The negative region of the latitudinal gradient of $\overline{q}$ disappears in the time mean state owing to the vorticity redistribution by the waves generated by the barotropic instability, and $\langle\overline{q}\rangle$ is nearly constant in midlatitudes. When the zonal mean zonal wind in high latitudes is stronger than the mean state, it is weaker in midlatitudes, or vice versa. In other words, when the gradient of PV in high latitudes is larger than the mean state, it is smaller in midlatitudes, or vice versa.

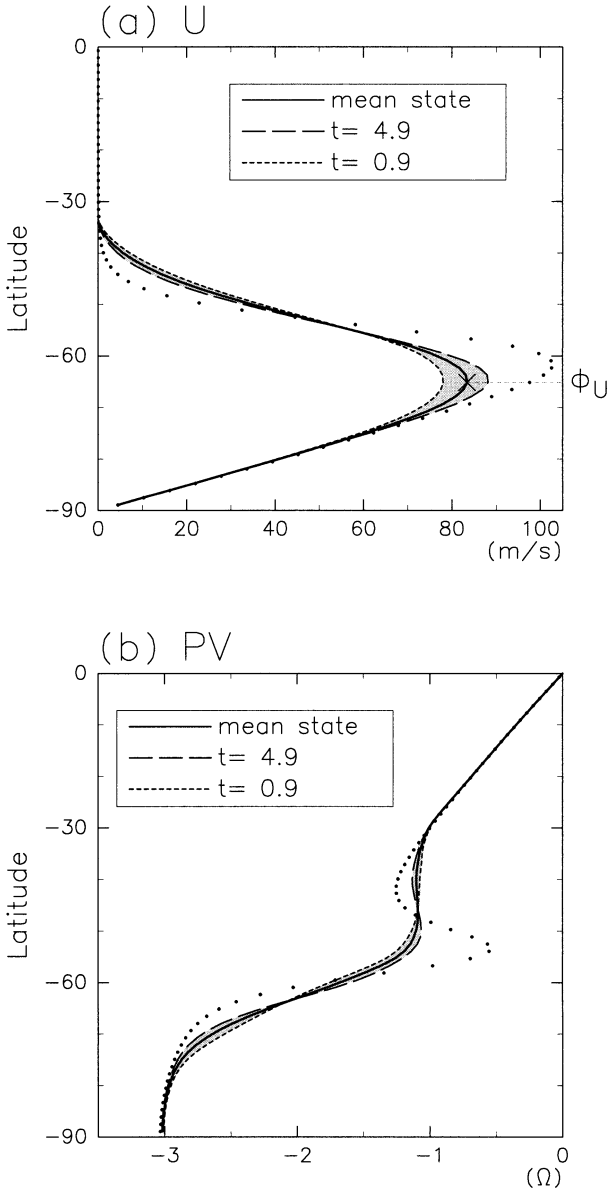

FIG. 10. Latitudinal profiles of (a) zonal mean zonal wind and (b) zonal mean PV obtained from the barotropic model experiment with $B = 6°$ and $h_0 = 0.08H$. The solid line shows the time mean state along with the variation range (shaded region). The dotted line shows the prescribed zonal mean zonal flow forcing. The broken and dashed lines show the profiles when the zonal mean zonal wind at the jet core $\phi = 65.1°$S has its maximum ($t = 4.9$) and minimum ($t = 0.9$), respectively. The value of the PV is scaled by Ω.

Horizontal structures of the waves 1 and 2 (not shown) also have similar characteristics to the observations shown in Fig. 5 (top). The amplitudes of stationary wave 1 and traveling wave 2 have only one maximum at 63.7° and 60.9°S, respectively, while the traveling wave 1 has double maxima at 55.3° and 66.5°S with a node between the two latitudes.

Figure 11 displays the polar diagram of the complex amplitudes for wave 1 at the lower latitude of the one maximum of the traveling wave amplitude and (Fig. 11b) the higher latitude of the other maximum and (Fig. 11c) that for wave 2 at the latitude of its maximum amplitude, as well as (Fig. 11d) the time variation of the zonal mean zonal wind at the latitude of the jet core $\phi = 65.1°$S. Dominance of stationary wave 1 and traveling wave 2 resembles the observed state as shown in Fig. 8. This is a purely periodic solution, which has similar characteristics to the observed quasi-periodic variations as follows. 1) Transient wave 1 propagates eastward with the same period as wave 2, keeping the out-of-phase relation between the higher and lower latitudes; 2) the traveling wave 1 at the higher latitude and wave 2 at the latitude of its maximum amplitude are in phase with the stationary wave 1 almost simultaneously at $t = 0.9$ and 10.6; 3) the amplitude of the traveling wave 2 has its maximum at that time, whereas the traveling wave 1 at the higher latitude has a minimum amplitude when in phase or out of phase with the stationary wave 1; 4) the zonal mean zonal wind is weakest when the phase overlap occurs ($t = 0.9$ and 10.6). Furthermore, traveling wave 3 also propagates eastward with the same angular frequency as waves 1 and 2, and its amplitude variation is similar to that observed (not shown).

The EP flux and its divergence for the model experiment are shown in Figs. 12a–d, together with the time change of zonal mean zonal wind at 65.1° and 51.1°S (Fig. 12e). Here, $\mathbf{F}_k(0, F_{\phi_k}, 0)^{\mathrm{T}} = (0, -\overline{u_k v_k}, 0)^{\mathrm{T}}$. Features of the EP flux are also similar to the observational results. 1) The EP flux for wave 1, $\mathbf{F}_1$, changes its direction periodically associated with the phase relation between the stationary wave 1 and traveling wave 1, thus the dipole pattern of the divergence with a node around 60°S also changes its sign periodically; 2) $\mathbf{F}_2$ also changes its direction periodically in the opposite direction to $\mathbf{F}_1$ with the dipole pattern of the divergence as seen for the first half of the period in Fig. 9b; 3) $\mathbf{F}_3$ is small compared to the other two components but shows periodic change of its direction; 4) The EP flux divergence of the wave-1 component dominates the EP flux divergence for waves 1–3, which explains the anticorrelated time change of the zonal mean zonal wind between 65.1° (solid line) and 51.1°S (dashed line). Only one difference of the EP flux in the model experiment from the observation is that the EP flux for the waves 1–3 is always convergent between 55° and 60°S, which is due to the fact that the EP flux convergence of wave 2 there is larger than the divergence of wave 1. All the evidence presented here shows that the observed traveling waves 1 and 3 as described in the previous section are consistent with the traveling waves generated by the wave–wave interaction of the stationary wave 1 and the traveling wave 2.

4. Interannual variability

Returning to the observation data, interannual variability of the quasi-periodic variations of the polar vor-

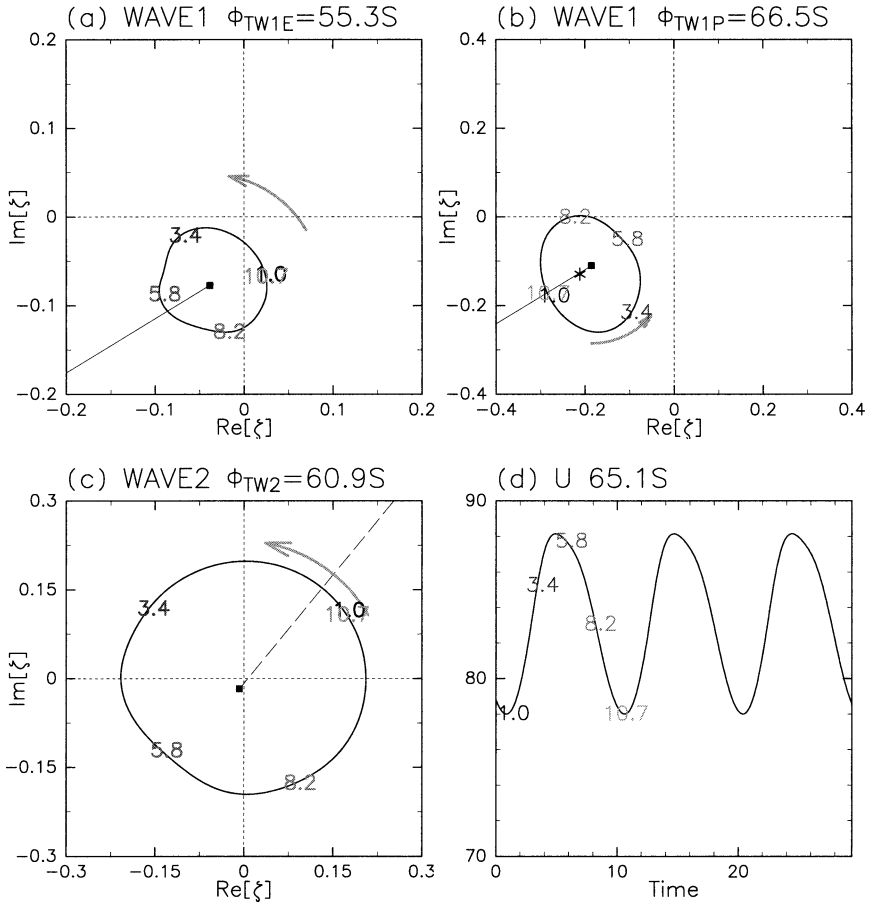

FIG. 11. Same as in Fig. 8, but for the model experiment.

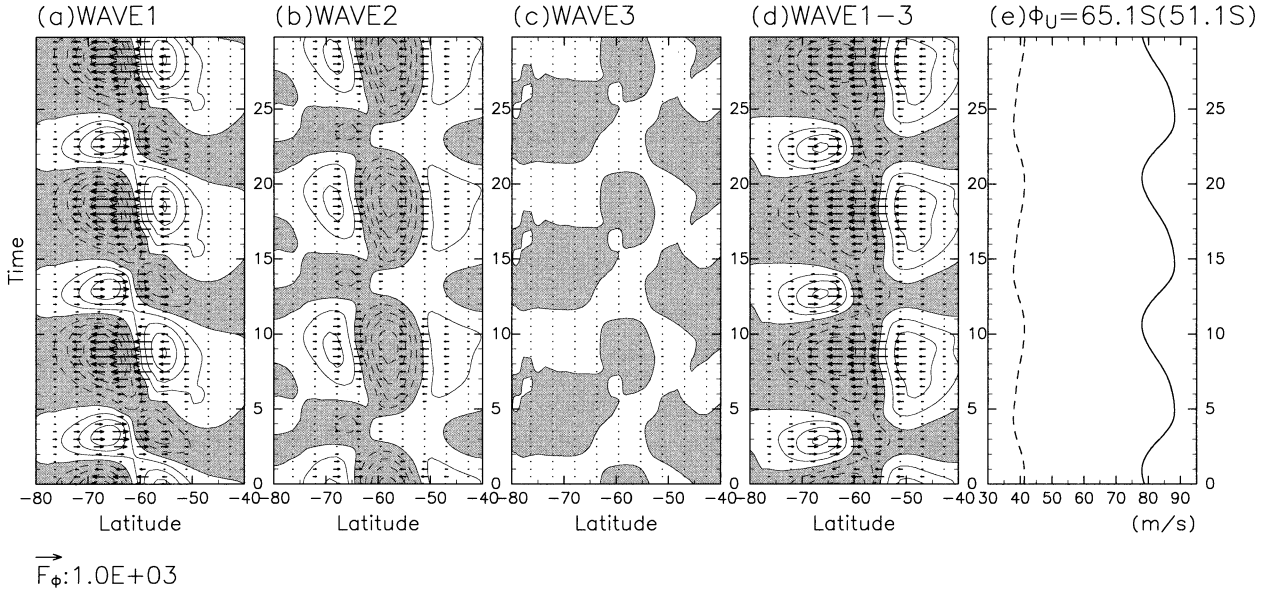

FIG. 12. (a)–(d) Same as in Fig. 9, but for 30 days for the model experiment. (a) The length of the unit vector is displayed under the graph. The contour interval is 0.8 m s^{-1} day^{-1}, and negative values are shaded. (e) Time evolution of the zonal mean zonal wind at 65.1° (solid line) and 51.1°S (dashed line) for the model experiment.

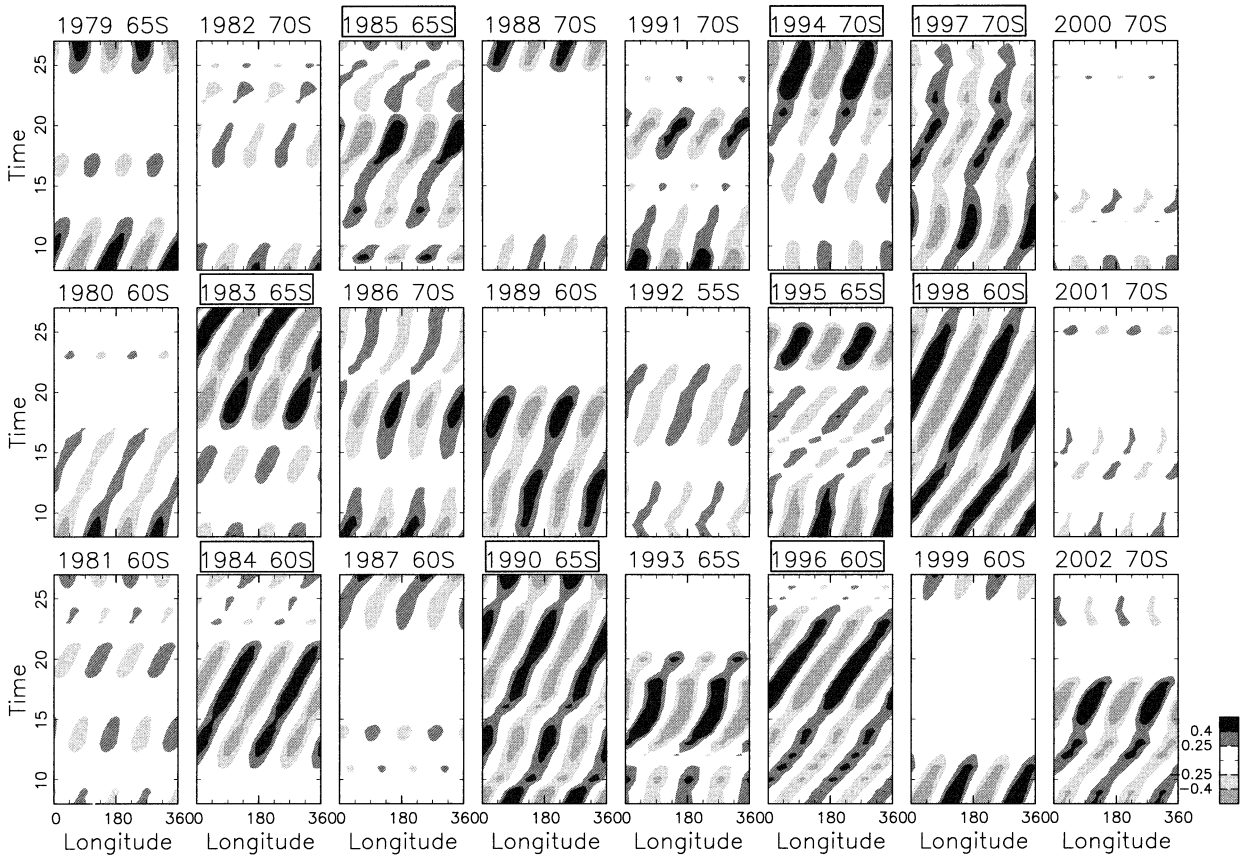

FIG. 13. Hovmöller diagrams of the traveling wave 2 at the maximum latitude for vorticity field at 20 hPa during 8 to 27 Oct for the 24 yr from 1979 to 2002. The value is scaled by Ω. The displayed latitude is the one where the time mean amplitude of the traveling wave 2 has its maximum and is denoted for each panel. The titles are enclosed by squares for the years in which the traveling wave 2 has the nine largest amplitudes.

tex is investigated using the 24-yr data from 1979 to 2002. Figure 13 shows Hovmöller diagrams of the traveling wave 2 at the latitude of its maximum amplitude (defined for each year and noted above each panel) for the 20-day period from 8 to 27 October in the 24 yr, which is the same period as Fig. 7 for the case of 1996. Regular eastward-traveling wave 2 with comparable amplitude to that in 1996 is often observed. The latitude of its maximum amplitude ranges from 55° to 70°S depending on the year.

Figure 14 shows the complex amplitudes for wave 1 at the higher-latitude maximum (solid line) and wave 2 at maximum latitude (dashed line) for eight of the years when the traveling wave 2 has a large amplitude: 1983, 1984, 1985, 1990, 1994, 1995, 1997, and 1998. For comparison, results for 1996 are shown in Fig. 8. Eastward propagation of the traveling wave 1 is clearly seen in 1983, 1984, and 1998 with the same phase relationship between the traveling waves 1 and 2. Traveling wave 1 tends to propagate eastward at a similar angular frequency as wave 2 and to be in phase with the stationary wave 1 nearly at the same timing with the phase overlap of wave 2 as seen in 1996. In particular, the amplitude variation in 1984 also shows similar characteristics with the case of 1996. In the other years shown in Fig. 14, the eastward propagation of wave 1 can be discernible for some subperiods, although the angular frequency is largely different. This kind of relationship is not clearly seen in the years when the amplitude of traveling wave 2 is small such as the years 1988, 2000, and 2001 (not shown).

Figure 15a shows the relation between the amplitude of the stationary wave 1 and that of the traveling wave 2 at the latitude of the maximum amplitude of each wave for the 24 yr. The stationary wave 1 has large interannual variability as reported by Hio and Hirota (2002), and its amplitude has a weak and negative correlation with that of the traveling wave 2 ($r = -0.39$). The amplitude of the stationary wave 1 for the 9 yr with large amplitude of the traveling wave 2 varies from year to year.

Figure 15b shows the scatter diagram between the amplitude of the traveling wave 2 and the latitudinal difference of the time mean zonal mean QGPV between 40° and 45°S at 20 hPa, where its latitudinal gradient is small (Fig. 1). For the 9 yr with the large amplitude, the latitudinal difference tends to be negative or small

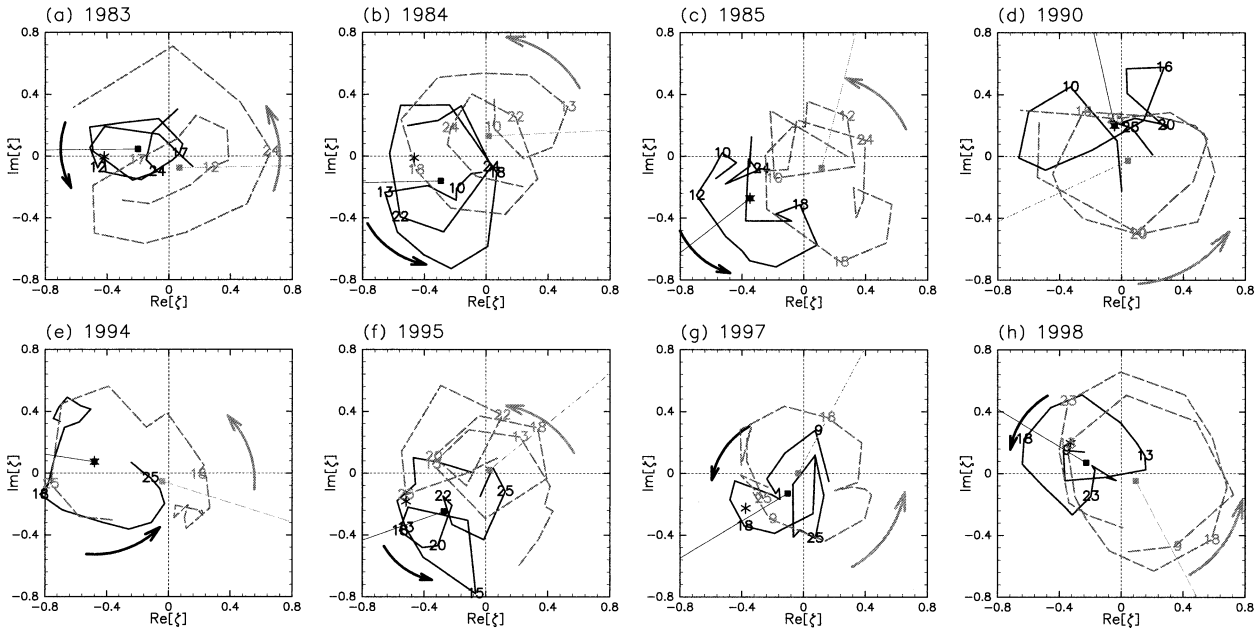

FIG. 14. Polar diagrams of the complex amplitude of wave 1 at the higher latitude of the maximum amplitudes (solid line) and wave 2 at the latitude of the maximum amplitude (dashed line) for the period of 20 days (a) from 8 to 27 Oct 1983, (b) 1984, (c) 1985, (d) 1990, (e) 1994, (f) 1995, (g) 1997, and (h) 1998. The marks are the same as in Fig. 8.

positive except for 1998. In 1986, for which the latitudinal gradient is also negative, the amplitude of the traveling wave 2 is not so small. Contrarily, the latitudinal difference of the time mean zonal mean QGPV tends to be large in other years with small amplitude of the traveling wave 2. These suggest the generation of traveling wave 2 by in situ instability of the zonal mean state when the amplitude of the traveling wave 2 is large except for 1998. In 1998, the wave activity flux from the troposphere is very large (Fig. 15d), suggesting that the traveling wave 2 is propagated from the troposphere in this year.

The relation of the amplitude of the traveling wave 2 to the horizontal component of the EP flux for wave 2 (F_{ϕ_2}) at 20 hPa between 50° and 70°S is shown in Fig. 15c. Since the horizontal component changes its sign periodically in the case of 1996 (Fig. 9), we take the time mean of the absolute value of F_{ϕ_2}. The horizontal component of the EP flux has a large magnitude for the 9 yr. On the other hand, the time mean of the vertical component of the EP flux for wave 2 at 100 hPa between 50° and 70°S has full range of variations for the 9 yr with large amplitude of the traveling wave 2 (Fig. 15d). In some of the years, for example, 1995 and 1997, the small wave activity propagated from the troposphere suggests the generation of traveling wave 2 in the stratosphere.

5. Discussion

In sections 2 and 4, we presented quasi-periodic variations of the polar vortex observed in October. The wave–wave interactions between the waves 1 and 2 were pointed out by Hirota et al. (1990) and Manney et al. (1991a) for August and September. Figure 16 shows the polar diagrams of the complex amplitudes of wave 1 (a) at 50° and (b) 65°S, and wave 2 (c) at 60°S for the period from 15 August to 20 September 1988, in which the quasi-periodic variation of these waves was reported by Hirota et al. (1990). We can find the similar periodic variations of the waves 1 and 2 and the zonal mean zonal wind as seen in Fig. 8 in spite of the slower phase speed.

Another case of the wave–wave interaction is found in the period from 8 August to 30 September 2002, during which, on 24 September, the polar vortex split in two and a major stratospheric sudden warming event occurred for the first time in over 2 decades of satellite observations (Allen et al. 2003). The polar diagrams of the complex amplitudes of wave 1 at (a) 50° and (b) 70°S, and wave 2 at (c) 60°S are shown in Fig. 17. As pointed out by Scaife et al. (2005) quasi-periodic variation of waves 1 and 2, and the zonal mean zonal wind (d) can be seen through the winter. Clustering of the dates written in black or gray shows that the eastward-traveling wave 1 at 70°S has a similar angular frequency to the wave 2 at 60°S and is anticorrelated with that at 50°S. The clustering also shows that phase overlap of traveling waves 1 and 2 with the stationary wave 1 occurs roughly at the same time. These phase variations similar to those in Figs. 8 and 11 suggest that the quasi-periodic variation of the polar vortex before its split can be understood as a result of the wave–wave interaction

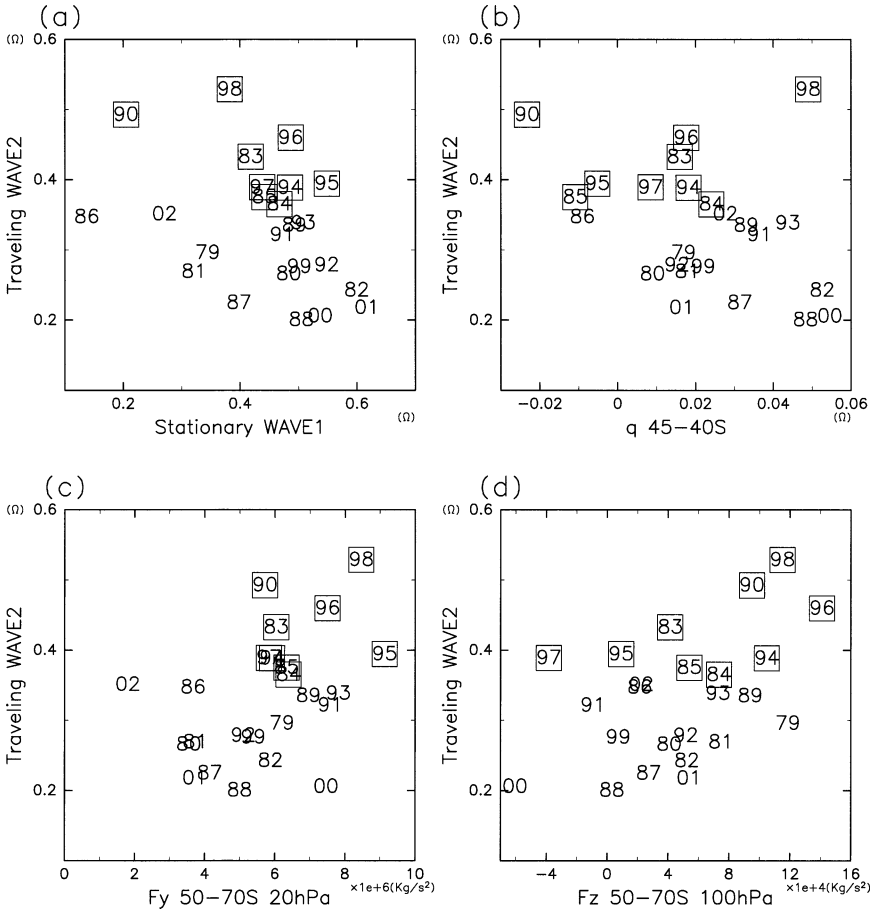

FIG. 15. (a) Scatter diagrams of the amplitude of the stationary wave 1 at 20 hPa at the latitude where the amplitude has its maximum value vs the time mean amplitude of traveling wave 2 at 20 hPa at the latitude where the amplitude is maximum, (b) the difference of the time mean zonal mean QGPV between 40° and 45°S at 20 hPa, (c) the time mean absolute value of the horizontal component of the EP flux of wave 2 between 50° and 70°S at 20 hPa, and (d) the time mean vertical component of the EP flux of wave 2 between 50° and 70°S at 100 hPa for the period of 20 days from 8 to 27 Oct for each year from 1979 to 2002. Each year is indicated by the last two digits. The meaning of the frame to select the 9 yr is the same as in Fig. 13.

between the stationary wave 1 and the traveling wave 2. This result is consistent with that by Manney et al. (2005): They made sensitivity tests using a mechanistic model with a time-varying bottom forcing near the tropopause analyzed at the Met Office and suggested that the vacillation of the wave amplitude may arise from the wave–wave interaction between the waves 1 and 2. Quasi-periodic variations of the polar vortex are sometimes observed in September in the other years, although the wave–wave interaction is not as clear as those in October due to slower phase speed of traveling wave 2. Seasonal evolution of the polar vortex and strong wave activity propagated from the troposphere obscure the interaction. The angular frequency of the traveling wave 2 is much larger in 2002 than in 1988, which may be a result of much earlier seasonal evolution in August and September 2002 (Hio and Yoden 2005).

6. Conclusions

Quasi-periodic variations of the polar vortex in the Southern Hemisphere stratosphere as shown in Fig. 2 were investigated from a viewpoint of the wave–wave interaction between wave 1 and wave 2. In a typical period for the 20 days from 8 to 27 October 1996, the traveling wave 1 propagates eastward with comparable amplitude to the stationary wave 1 and the eastward-traveling wave 2 (Figs. 3 and 4). This traveling wave 1 has a latitudinal node around 60°S where both the stationary wave 1 and the traveling wave 2 have maximum amplitude (Fig. 5). The EP flux diagnosis shows that the traveling wave 1 is generated in the stratosphere (Fig. 6b).

Hovmöller diagrams (Fig. 7) and the polar diagrams of the complex amplitude (Fig. 8) reveal that traveling waves 1 and 2 have the same angular frequency of about

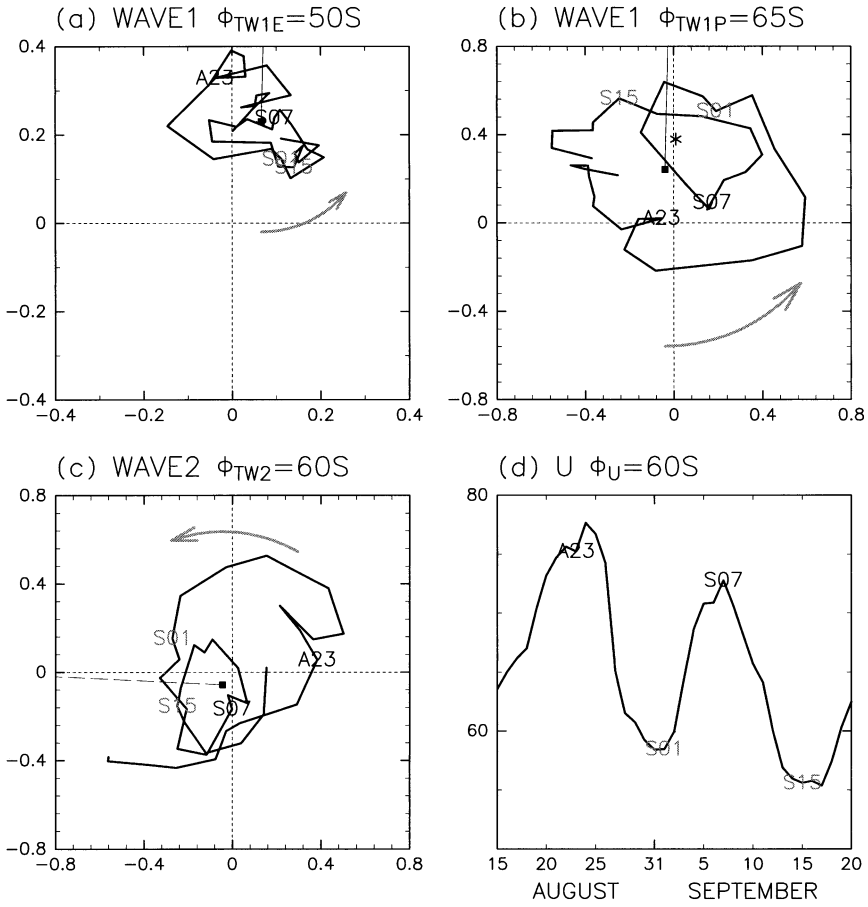

FIG. 16. Same as in Fig. 8, but for the period of 37 days from 15 Aug to 20 Sep 1988. The latitude is defined in the same way as Fig. 8 and is specified at the top of each panel. The labels indicate the initials of the months and dates.

60° day^{-1}. The traveling wave 1 in high latitudes and the traveling wave 2 are in phase with the stationary wave 1 at the same time. The amplitude of the traveling wave 2 is a maximum at this time, while the traveling wave 1 has a minimum amplitude when it is in phase or out of phase with the stationary wave 1. The zonal mean zonal wind also vacillates quasi-periodically and has its minimum when the above-mentioned phase overlapping occurs.

The EP flux for wave 1 in the middle stratosphere also shows quasi-periodic variations due to interference between the stationary and traveling components (Fig. 9). The horizontal component changes its direction with the period of the eastward propagation and the divergence of the EP flux changes quasi-periodically. As the wave driving of the wave 1 component dominates, the zonal mean zonal wind also changes quasi-periodically through the wave–mean-flow interaction.

Similar periodic variations of the polar vortex are obtained in the numerical experiment with a spherical barotropic model in the circumstance that the stationary wave 1 generated by the topographic forcing coexists with the eastward-traveling wave 2 due to barotropic instability of the forced mean zonal wind. The traveling wave 1 with a node in midlatitude, which is generated through the wave–wave interaction, propagates eastward at the same angular frequency as the traveling wave 2 (Fig. 11). The phase relationship and the amplitude fluctuation of these waves show the same characteristics with the observation. Furthermore, the zonal mean zonal wind vacillates with the same frequency, which is explained by the wave interference between the stationary wave 1 and the traveling wave 1 (Fig. 12). These results support that the observed quasi-periodic variations of the polar vortex can be explained by the wave–wave interaction between the stationary wave 1 and the eastward-traveling wave 2.

In 9 out of the 24 yr, from 1979 to 2002, similar quasi-periodic variations of the polar vortex are seen for the same 20 days in October (Figs. 13 and 14). The amplitude of the stationary wave 1 and that of the traveling wave 2 are large in these years (Fig. 15a). The amplitude of the wave 2 is well correlated with the latitudinal gradient of the zonal mean quasigeostrophic potential vorticity in midlatitudes (Fig. 15b).

It is important to know the latitudinal structures of

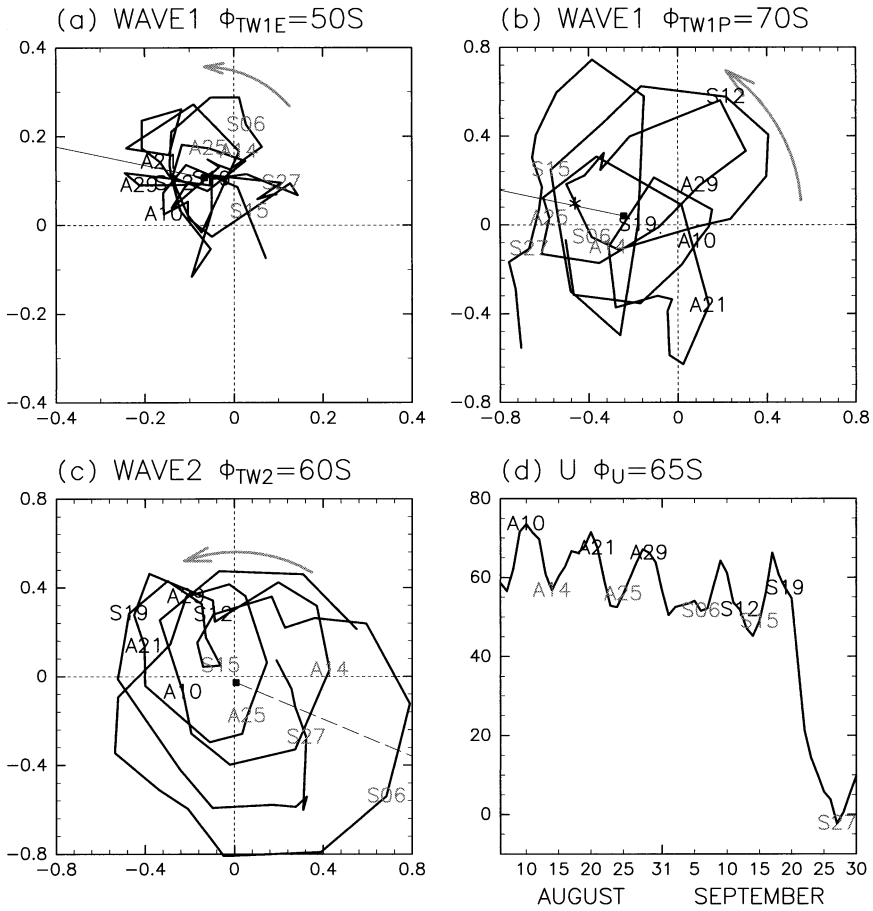

FIG. 17. Same as in Fig. 16, but for the period of 55 days from 6 Aug to 30 Sep 2002.

waves and zonal mean quantities in diagnosing wave–wave interaction. The nodal structure of the traveling wave 1 is the evidence to show the occurrence of the wave–wave interaction. Therefore, if we look at the amplitude of waves 1 and 2 only at 60°S as in some previous studies, it would be difficult to find a clear relationship between the waves 1 and 2 because the node of the traveling wave 1 is located around 60°S and the latitude shifts from year to year.

Acknowledgments. We thank Dr. K. Ishioka for his efficient library package of the spherical barotropic model with the spectral transform method (Ishioka 2002). We also thank Dr. R. Mizuta for providing the source program used in Mizuta and Yoden (2001). We also thank three anonymous reviewers for helpful comments. This research was partially supported by the Kyota University Active Geosphere Investigations for the 21st Century COE (KAGI 21), which was approved by the Ministry of Education, Culture, Sports, Science, and Technology (MEXT) of Japan. The GFD-DENNOU library (SGKS Group 2001) was used for graphical output.

REFERENCES

Allen, D. R., R. M. Bevilacqua, G. E. Nedoluha, C. E. Randall, and G. L. Manney, 2003: Unusual stratospheric transport and mixing during the 2002 Antarctic winter. *Geophys. Res. Lett.*, **30,** 1599, doi:10.1029/2003GL017117.

Andrews, D. G., J. R. Holton, and C. B. Leovy, 1987: *Middle Atmosphere Dynamics.* Academic Press, 489 pp.

Hartmann, D. L., 1979: Baroclinic instability of realistic zonal-mean states to planetary waves. *J. Atmos. Sci.,* **36,** 1141–1154.

——, 1983: Barotropic instability of the polar night jet stream. *J. Atmos. Sci.,* **40,** 817–835.

——, C. R. Mechoso, and K. Yamazaki, 1984: Observations of wave–mean flow interaction in the Southern Hemisphere. *J. Atmos. Sci.,* **41,** 351–362.

Harwood, R. S., 1975: The temperature structure of the Southern Hemisphere stratosphere August–October 1971. *Quart. J. Roy. Meteor. Soc.,* **101,** 75–91.

Hio, Y., and I. Hirota, 2002: Interannual variations of planetary waves in the Southern Hemisphere stratosphere. *J. Meteor. Soc. Japan,* **80,** 1013–1027.

——, and S. Yoden, 2005: Interannual variations of the seasonal march in the Southern Hemisphere stratosphere for 1979–2002 and characterization of the unprecedented year 2002. *J. Atmos. Sci.,* in press.

Hirooka, T., 1986: Influence of normal mode Rossby waves on the mean field: Interference with quasi-stationary waves. *J. Atmos. Sci.,* **43,** 2088–2097.

Hirota, I., and Y. Sato, 1969: Periodic variation of the winter stratospheric circulation and intermittent vertical propagation of planetary waves. *J. Meteor. Soc. Japan*, **47,** 390–402.

——, K. Kuroi, and M. Shiotani, 1990: Midwinter warmings in the Southern Hemisphere stratosphere in 1988. *Quart. J. Roy. Meteor. Soc.,* **116,** 929–941.

Holton, J. R., and C. Mass, 1976: Stratospheric vacillation cycles. *J. Atmos. Sci.,* **33,** 2218–2225.

Ishioka, K., cited 2002: Ispack-0.61 (in Japanese). GFD-DENNOU Club. [Available online at http://www.gfd-dennou.org/arch/ispack/.]

——, and S. Yoden, 1995: Non-linear aspects of barotropically unstable polar vortex in a forced-dissipative system: Flow regimes and tracer transport. *J. Meteor. Soc. Japan,* **73,** 201–212.

Lighthill, J., 1978: *Waves in Fluid.* Cambridge University Press, 504 pp.

Manney, G. L., T. R. Nathan, and J. L. Stanford, 1988: Barotropic stability of realistic stratospheric jets. *J. Atmos. Sci.,* **45,** 2545–2555.

——, J. D. Farrara, and C. R. Mechoso, 1991a: The behavior of wave 2 in the Southern Hemisphere stratosphere during late winter and early spring. *J. Atmos. Sci.,* **48,** 976–998.

——, C. R. Mechoso, L. S. Elson, and J. D. Farrara, 1991b: Planetary-scale waves in the Southern Hemisphere winter and early spring stratosphere: Stability analysis. *J. Atmos. Sci.,* **48,** 2509–2523.

——, and Coauthors, 2005: Simulations of dynamics and transport during the September 2002 Antarctic major warming. *J. Atmos. Sci.,* in press.

Mechoso, C. R., A. O'Neill, V. D. Pope, and J. D. Farrara, 1988: A study of stratospheric final warming of 1982 in the Southern Hemisphere. *Quart. J. Roy. Meteor. Soc.,* **114,** 1365–1384.

Mizuta, R., and S. Yoden, 2001: Chaotic mixing and transport barriers in an idealized stratospheric polar vortex. *J. Atmos. Sci.,* **58,** 2615–2628.

Randel, W. J., 1987: A study of planetary waves in the southern winter troposphere and stratosphere. Part I: Wave structure and vertical propagation. *J. Atmos. Sci.,* **44,** 917–935.

Robinson, W. A., 1985: A model of the wave 1–wave 2 vacillation in the winter stratosphere. *J. Atmos. Sci.,* **42,** 2289–2304.

Rong, P. P., and D. W. Waugh, 2004: Vacillations in a shallow water model of the stratosphere. *J. Atmos. Sci.,* **61,** 1174–1185.

Salby, M., and R. Garcia, 1987: Vacillations induced by interference of stationary and traveling planetary waves. *J. Atmos. Sci.,* **44,** 2679–2711.

Scaife, A. A., and I. N. James, 2000: Response of the stratosphere to interannual variability of tropospheric planetary waves. *Quart. J. Roy. Meteor. Soc.,* **126,** 275–297.

——, D. R. Jackson, R. Swinbank, N. Batchart, H. E. Thornton, M. Keil, and L. Henderson, 2005: Stratospheric vacillations and the major warming over Antarctica in 2002. *J. Atmos. Sci.,* in press.

Scinocca, J. F., and P. H. Haynes, 1998: Dynamical forcing of stratospheric planetary waves by tropospheric baroclinic eddies. *J. Atmos. Sci.,* **55,** 2361–2392.

SGKS Group, cited 2001: DCL-5.2 (in Japanese). GFD-DENNOU Club. [Available online at http://www.gfd-dennou.org/library/dcl/.]

Shiotani, M., K. Kuroi, and I. Hirota, 1990: Eastward traveling waves in the Southern Hemisphere during the spring of 1983. *Quart. J. Roy. Meteor. Soc.,* **116,** 913–927.

Smith, A. K., 1983: Observation of wave–wave interactions in the stratosphere. *J. Atmos. Sci.,* **40,** 2486–2496.

——, J. C. Gille, and L. V. Lyjak, 1984: Wave–wave interactions in the stratosphere: Observations during quiet and active wintertime periods. *J. Atmos. Sci.,* **41,** 363–373.

Ushimaru, S., and H. Tanaka, 1992: A numerical study of the interaction between stationary Rossby waves and eastward-traveling waves in the Southern Hemisphere stratosphere. *J. Atmos. Sci.,* **49,** 1354–1373.

Yoden, S., 1987: Bifurcation properties of a stratospheric vacillation model. *J. Atmos. Sci.,* **44,** 1723–1733.

Young, R., and H. Houben, 1989: Dynamics of planetary-scale baroclinic waves during Southern Hemisphere winter. *J. Atmos. Sci.,* **46,** 1365–1383.